Atomically dispersed Mn doped Ru@RuO2 core/shell nanostructure with multiple synergies for efficient acidic water electrolysis

Haibin Ma[a‡], Jun Zhou[b‡], Yang Zhao[c], Zhiwei Hu[d], Jiwei Ma[a*], Hongfei Cheng[a*]

a. *Shanghai Key Laboratory for R&D and Application of Metallic Functional Materials, Institute of New Energy for Vehicles, School of Materials Science and Engineering, Tongji University, Shanghai 201804, P. R. China.*

b. *Institute of Materials Research and Engineering (IMRE), Agency for Science, Technology and Research (A*STAR), 2 Fusionopolis Way, Innovis #08-03, Singapore 138634, Republic of Singapore.*

c. *Dalian National Laboratory for Clean Energy (DNL), Dalian Institute of Chemical Physics, Chinese Academy of Science, Dalian 116023, P. R. China.*

d. *Max Planck Institute for Chemical Physics of Solids, Nöthnitzer Strasse 40, 01187 Dresden, Germany.*

‡ These authors contributed equally to this work.

* Corresponding authors: jiwei.ma@tongji.edu.cn; cheng_hongfei@tongji.edu.cn

Abstract

The high overpotential and unsatisfactory stability of RuO_2-based catalysts seriously hinder their application in acidic oxygen evolution reaction (OER) electrolysis. Herein, we report a Mn single-atom doped Ru@RuO_2 catalyst with core/shell structure, denoted as Ru@Mn-RuO_2, which exhibits a much low overpotential of 177 mV at the current density of 10 mA cm^{-2} and an excellent stability of 360 hours as compared with Ru@RuO_2. Detailed structural characterizations confirm that single Mn atom is homogeneously dispersed in RuO_2 shell, which causes lattice contraction of RuO_2. The enhanced OER activity by Mn doping is attributed to multiple synergistic effects. These include the MnO_x-Ru (oxide shell) synergy, MnO_x-Ru (metal core) synergy, and the Ru (core)-RuO_2 (shell) synergy. Furthermore, experimental and theoretical studies prove that Mn single-atom doping leads to lattice contraction of RuO_2 shell, namely a reduced reaction pathway in RuO_2 shell, thus an improved OER activity and stability was obtained.

Keywords: Single-atom doping, core/shell structure, lattice contraction, acidic oxygen evolution reaction, multiple synergistic effects

Introduction

Water electrolysis using sustainable electricity is a highly promising technology to produce green hydrogen in the near future.[1-2] Generally, electrocatalytic water splitting can be performed in acidic, alkaline, or neutral electrolytes.[3-5] Alkaline water electrolysis technology is currently dominant in industry, but it has some drawbacks, such as crossover of gaseous products, high ohmic resistance, limited current density and low operating pressure. In contrast, proton exchange membrane (PEM) water electrolyzers[6-8] can overcome these issues,[9-10] making them a promising next-generation green hydrogen producing technology[11] that has garnered world-wide interests in this field. However, the overall efficiency of PEM water electrolyzers is limited by the sluggish oxygen evolution reaction (OER) at the anode. Ruthenium dioxide (RuO_2), as a benchmark OER electrocatalyst,[12-13] suffers from high reaction overpotentials, and easy transformation of surface stable Ru^{4+} to dissolvable $Ru^{n>4+}$ species in acidic media.[14-16] This greatly degrades its performance over long-time operation. There is an urgent need, though it remains a significant challenge, to develop highly active and stable Ru-based catalysts for acidic water splitting.

The past decades have witnessed the effectiveness of introducing synergistic effect associated with lattice distortion to improve catalytic performance.[15,17-20] Constructing Ru-based hetero-interfaces with core/shell structures, such as $Ru@RuO_2$, could be an approach to introduce synergistic effect.[21-22] It should be noted that the synergistic effect induced by core-shell structure is most significant in the atomic layers adjacent to the interface and rapidly diminishes as it moves toward the surface layer, where catalytic reactions occur. This implies that the synergistic effect is limited in core/shell structure, particularly for those with thick shells. Fortunately, the limitations of core/shell structure can be mitigated by homogenously dispersing dopant atoms within the thin shell. In addition, dopant engineering, especially choosing cationic heteroatoms as highly dispersed single-atomic sites to substitute Ru, can also modulate electronic structure of oxidized Ru sites[23-24] by multiple synergistic effect. These effects arise from lattice distortion caused by single metal doped RuO_2 shell, single metal dopant with the core, and the physical merits of core/shell heterostructure itself. This approach effectively resists the overoxidation of RuO_2 during acidic OER process.

Based on the above considerations, we design a core/shell catalyst composed of a RuO_2 shell doped with manganese (Mn) single atoms and a metallic Ru core for acidic water splitting. The impact of Mn doping is impressive: the pristine $Ru@RuO_2$ core/shell heterostructure requires an overpotential of 261 mV and has a durability of less than 40 hours at a current density of 10 mA cm^{-2}, while the as-fabricated $Ru@Mn\text{-}RuO_2$ catalyst with a similar structure,

requires an overpotential of only 177 mV to drive the same current density for nearly 360 hours. Density functional theory (DFT) studies confirm that Mn single-atom doping induces lattice contraction of tetragonal RuO_2, effectively modulates the electronic structure of RuO_2, and enhances the catalytic activity and stabilization of RuO_2.

Synthesis and structure of catalysts

We developed a two-step process to fabricate core/shell Ru@Mn-RuO_2 heterostructure. Briefly, wet impregnation of metal precursors was adopted to form the alginate hydrogel, followed by annealing in air to yield the final product. The transmission electron microscopy (TEM) image in Figure 1a shows the formation of core/shell spherical morphology with the shell thickness of about 1 nm. The X-ray diffraction (XRD) patterns in Figure 1b display the characteristic peaks of crystalline hexagonal Ru (JCPDS 06-0663) and tetragonal RuO_2 (JCPDS 43-1027) phases, with no other unidentified peaks present. The XRD refinement indicates lattice contraction (Figure 1b, Figure S1 and Table S1) after introducing 2.01wt% (obtained from inductively coupled plasma mass spectroscopy (ICP-MS) and shown in Table S2) of Mn species compared with the control sample Ru@RuO_2 (Figure S2). The high-angle annular dark-field scanning TEM (HAADF-STEM) images and the corresponding fast Fourier transformed (FFT) pattern in Figure 1c-e show Mn atoms are dispersed on the (101) planes of tetragonal RuO_2 shell, representatively. The STEM image in Figure S3 further demonstrates that Mn atoms are doped in RuO_2 phase. The energy-dispersive spectroscopic (EDS) mappings in Figure 1f indicate the homogeneous dispersion of Mn atoms.

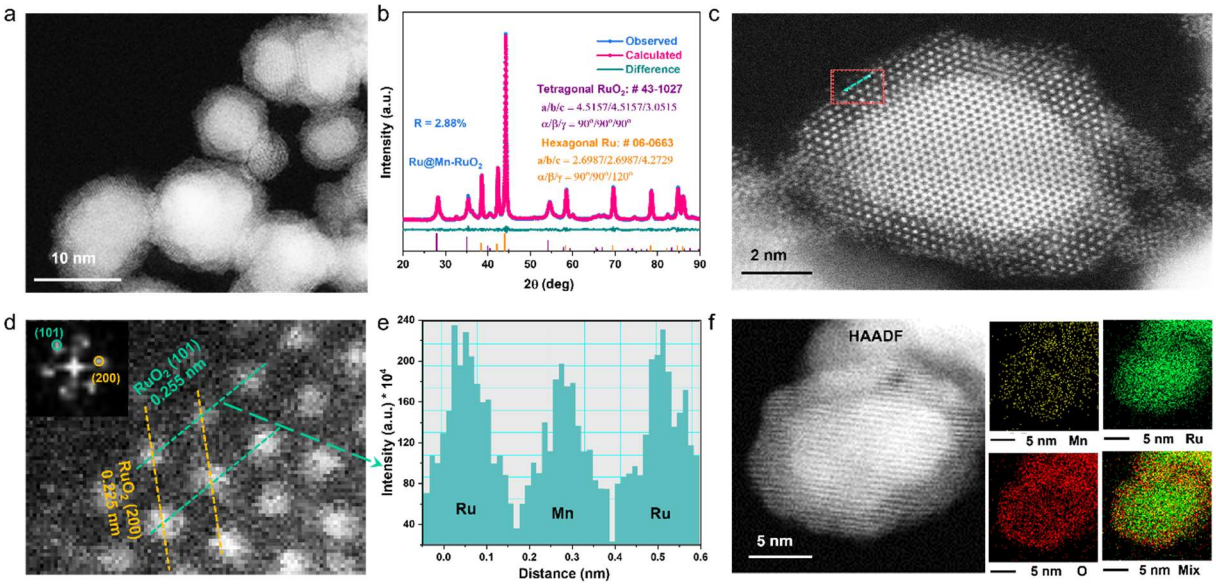

Figure 1. **Synthesis and characterization of Ru@Mn-RuO_2 heterostructure**. a, TEM image of Ru@Mn-RuO_2 catalyst. b, Refined XRD pattern of Ru@Mn-RuO_2 heterostructure. c, HAADF-STEM image of Ru@Mn-RuO_2 core/shell heterostructure. d, The enlarged image of

the area enclosed within red dashed rectangle in c and the corresponding FFT pattern (inset). e, The integrated pixel intensity along the green dashed line in c. f, EDS mapping images of Ru@Mn-RuO_2 catalyst, in which green, red, and yellow represents Ru L, O K, and Mn L, respectively.

Electronic properties of catalysts

The electronic properties of Ru@Mn-RuO_2 catalyst were firstly investigated by X-ray photoelectron spectroscopy (XPS). There are six peaks in the high-resolution Mn 2p XPS spectrum (Figure 2a) of Ru@Mn-RuO_2. Peaks at 641.43 and 653.28 eV are assigned to the Mn $2p_{3/2}$ and Mn $2p_{1/2}$ of Mn^{2+}, respectively, peaks at 643.87 and 656.16 eV are assigned to the Mn $2p_{3/2}$ and Mn $2p_{1/2}$ of Mn^{3+}, and those at 646.93 and 658.90 eV are ascribed to the Mn $2p_{3/2}$ and Mn $2p_{1/2}$ of Mn^{4+}.[25-27] The high-resolution Ru 3d XPS spectra (Figure 2b) show two sets of doublet peaks between 278 and 291 eV, which could be attributed to the doublet peaks of Ru^0 $3d_{5/2}$, $3d_{3/2}$ and Ru^{4+} $3d_{5/2}$, $3d_{3/2}$.[28-30] The binding energies of Ru^{4+} $3d_{5/2}$ and Ru^0 $3d_{5/2}$ for Ru@Mn-RuO_2 positively shift by around 0.10 eV and 0.11 eV compared with those of Ru@RuO_2, respectively, suggesting that Ru in the Ru@Mn-RuO_2 catalyst possesses a higher oxidation state than that in Ru@RuO_2. The peak shifts of Ru 3d XPS spectra indicate the existence of multiple synergistic effects after Mn doping, including the MnO_x with Ru species in the thin RuO_2 shell and MnO_x with Ru species in the inner Ru core. The above XPS analysis indicates the electronic structure of tetragonal RuO_2 in Ru@Mn-RuO_2 is efficiently modulated by incorporating Mn species.

X-ray absorption near edge structure (XANES) spectra and the extended X–ray absorption fine structure (EXAFS) at the 3d and 4d transition metal elements are powerful experimental techniques to explore the electronic structure[31-33] and local environment[34-36] of the interested elements, respectively. We have measured and analyzed XANES and EXAFS spectra of Ru K-edge for both Ru@Mn-RuO_2 and Ru@RuO_2 core/shell heterostructures (Figure 2c, d and Figure S4). The XANES results in Figure 2c suggest that Ru ion in Ru@Mn-RuO_2 possess higher valence state compared with that in Ru@RuO_2, consistent with the XPS results. The Ru K-edge EXAFS spectrum of Ru@Mn-RuO_2 exhibits the Ru-O peak at approximately 1.5 Å (Figure 2d), which shifts to shorter distance compared with that of Ru@RuO_2, further indicating the lattice contraction in Ru@Mn-RuO_2 after Mn doping and consistent with the XRD refinement analysis. The Mn K-edge XANES spectrum suggests the Mn oxidation state in Ru@Mn-RuO_2 is between Mn^{3+} of Mn_2O_3 and Mn^{4+} of MnO_2, approaching the valence state value of +3.21, (Figure 2e and Figure S5). The corresponding EXAFS spectrum of Ru@Mn-RuO_2 at the Mn K-edge shows a dominant peak at around 1.5 Å (Figure 2f), which is assigned

to the Mn-O coordination. And the slightly protruded peak of the Mn-K EXAFS in Ru@Mn-RuO_2 locating approaching at 3.3 Å is assigned to the Mn-Ru coordination. No obvious Mn-Mn bonds are observed in Ru@Mn-RuO_2, as suggested by the distinct EXAFS spectrum compared with commercial MnO_2, commercial Mn_2O_3 and Mn foil as references. This indicates the atomic dispersion of Mn within the lattice of RuO_2 shell. The XAS analysis above clearly suggests Mn atoms are mainly uniformly distributed in the RuO_2 lattice.

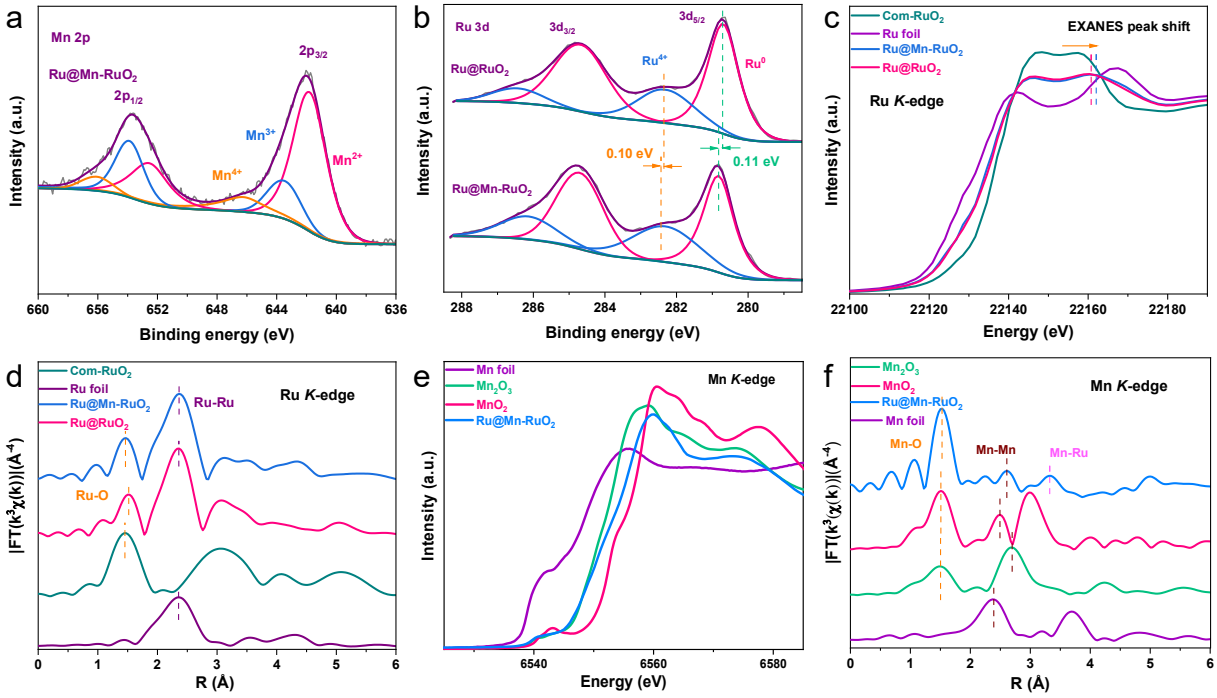

Figure 2. Electronic structure of Ru@Mn-RuO_2 and Ru@RuO_2 heterostructures. a, b, High-resolution XPS spectra of Mn 2p (a) and Ru 3d (b). c, d, XANES (c) and EXAFS (d) spectra of the Ru-K edge for commercial RuO_2, Ru foil, Ru@Mn-RuO_2 and Ru@RuO_2 heterostructures. e, f, XANES (e) and EXAFS (f) spectra at the Mn-K edge of Mn_2O_3, MnO_2, Ru@Mn-RuO_2, and Mn foil.

Electrochemical characterization in acidic electrolyte

Following OER standard measurements,[13,15,37] we first evaluated OER activities of Ru@Mn-RuO_2 heterostructure and other control samples using a standard rotating disk electrode (RDE) set-up. The control samples include Ru@RuO_2 heterostructure and commercial RuO_2 nanoparticles (Com-RuO_2). Linear sweep voltammetry (LSV) curves (Figure 3a) show that our as-synthesized Ru@RuO_2 heterostructure presents better OER activity than commercial RuO_2, mainly ascribed to the formation of hetero-interface. The commercial RuO_2 catalyst requires the overpotential of 335 mV (Figure 3b) to deliver the current density of 10 mA cm^{-2}, consistent with previous reports.[15,38] We explored the influence of Mn doping concentration on the electrocatalysis of Ru@Mn-RuO_2. As shown in Figure S6, the sample with

a Mn doping concentration of 2.01wt% exhibited best performance compared with other contrast samples. This suggests that the optimum mass of Mn precursor in the synthesis procedure is 10 mg. Incorporating Mn single atoms into the tetragonal RuO_2 shell significantly enhances the OER performance, yielding an overpotential of 177 mV at 10 mA cm^{-2}, much lower than that of Ru@RuO_2 (261 mV). This indicates the effectiveness of forming multiple synergistic effects, including single atomic Mn with Ru species in the thin RuO_2 shell, single atomic Mn with Ru species in metallic Ru core, and the core/shell heterostructure itself. Furthermore, the overpotential difference further increased rapidly with the increase of current densities, due to the significantly reduced Tafel slope of Ru@Mn-RuO_2 (58.5 mV dec^{-1}) compared with Ru@RuO_2 (78.3 mV dec^{-1}) and commercial RuO_2 (82.6 mV dec^{-1}) (Figure 3c). Electrochemical impedance spectroscopy (EIS) of Ru@Mn-RuO_2 at the overpotential of 150 mV shows the lowest charge transfer resistance (Figure S7), suggesting enhanced OER kinetics compared with Ru@RuO_2 and commercial RuO_2.[28,38] The superior activity of Ru@Mn-RuO_2 is among the best compared with other recently reported representative acidic OER catalysts (Figure 3d and Table S3).

To better understand the origin of the superior OER performance of Ru@Mn-RuO_2, we first tested the electrochemical double layer capacitance (C_{dl}) (Figure S8) to calculate the electrochemical active surface area (ECSA) for intrinsic activity normalization. Our prepared Ru@Mn-RuO_2 and Ru@RuO_2 core/shell structures clearly show higher C_{dl} (Figure 3e) and ECSA than those of commercial RuO_2. In particular, Ru@Mn-RuO_2 has the highest C_{dl} and ECSA, more than twice those of Ru@RuO_2, suggesting that the incorporation of Mn single atoms can significantly increase the number of active sites. The ECSA-normalized OER activity, namely specific activity, also follows the order Ru@Mn-RuO_2 > Ru@RuO_2 > Com-RuO_2 (Figure 3f), indicating intrinsic OER activity of Ru@Mn-RuO_2 core/shell heterostructure is improved due to the incorporation of atomic Mn dopants to tetragonal RuO_2 shell. We then evaluated the Faradaic efficiency (FE) of Ru@Mn-RuO_2 catalyst. As shown in Figure S9, the calculated FE is approaching 96%, indicating excellent selectivity of Ru@Mn-RuO_2 toward acidic OER.

The effects of other 3d transition metals as dopants, including Co and Fe, on the performance of Ru@RuO_2 core/shell heterostructure towards acidic OER are also investigated. The Ru@Co-RuO_2 (Figure S10 and Figure S11), and Ru@Fe-RuO_2 (Figure S12 and Figure S13) core/shell heterostructures with different lattice distortion degree were prepared using the same method with Ru@Mn-RuO_2. The standard RDE test results confirmed that Mn is the optimum dopant (Figure S14).

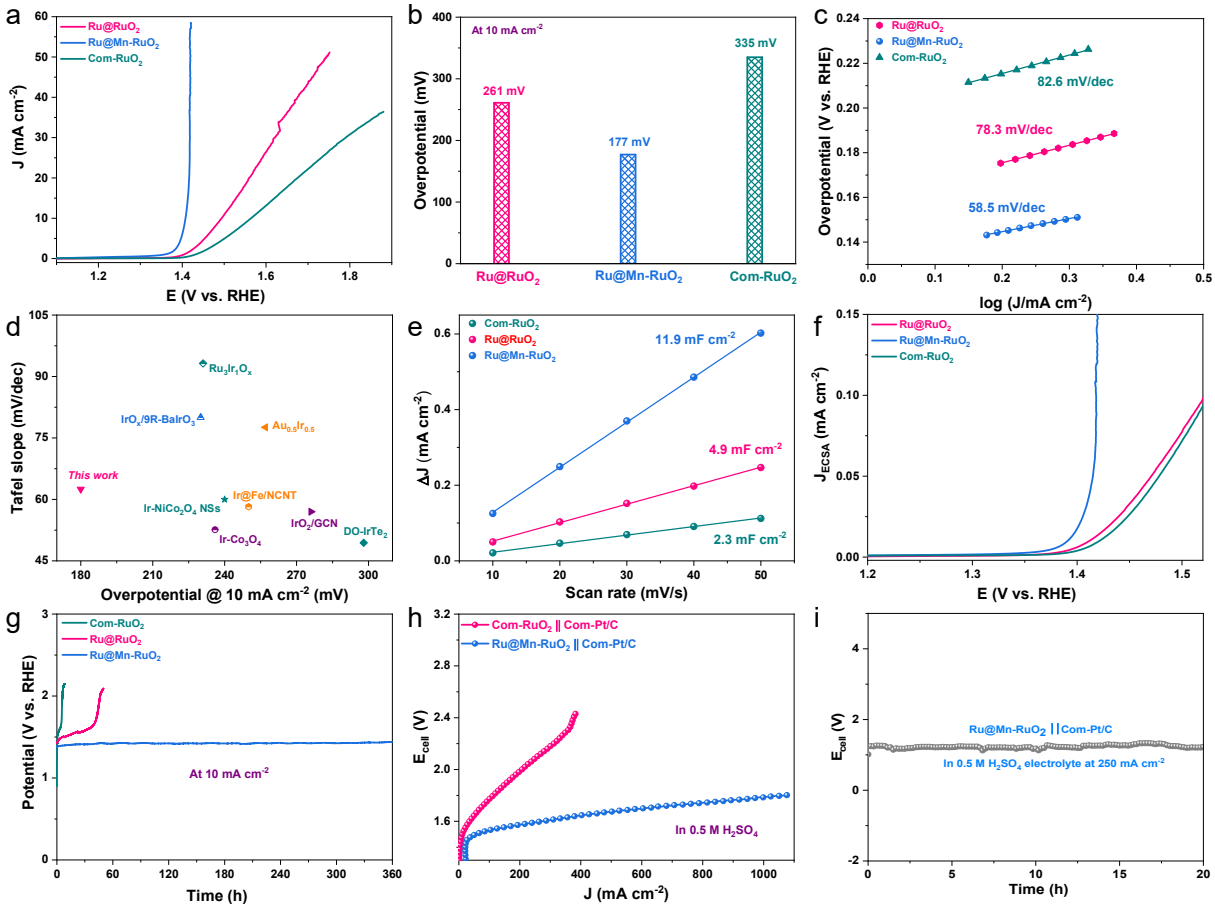

Figure 3. **Acidic OER performance**. a, b, c, LSV curves (a), Overpotentials at the current density of 10 mA cm^{-2} (b) and (c) Tafel slopes of Ru@Mn-RuO_2, Ru@RuO_2 and commercial RuO_2 catalysts. d, Comparison of the overpotentials and Tafel slopes with recently reported noble metal-based catalysts. e, C_{edl} plot derived from the CV curves. f, LSV curves normalized to the ECSA of Ru@Mn-RuO_2 and Ru@RuO_2. g, OER stability measurements of Ru@Mn-RuO_2, Ru@RuO_2 and commercial RuO_2 catalysts. h, Comparison for the activity of Ru@Mn-RuO_2 || Com-Pt/C and Com-RuO_2 || Com-Pt/C electrolyzers in 0.5 M H_2SO_4 electrolyte. i, Stability evaluation of Ru@Mn-RuO_2 || Com-Pt/C electrolyzer at the current density of 250 mA cm^{-2}.

Apart from the excellent OER activity, good stability plays an even more important role in practical acidic water splitting electrolysis.[39-40] We investigated OER durability in acidic electrolyte at 10 mA cm^{-2} on the standard RDE system, a widely adopted benchmark criterion in literature.[15,41] Although our fabricated Ru@RuO_2 heterostructure shows improved stability compared with commercial RuO_2, its performance still degraded at a rapid rate and lasted no longer than 40 h (Figure 3g). This performance degradation was markedly mitigated after incorporation of Mn atoms. Our as-synthesized Ru@Mn-RuO_2 core/shell heterostructure presents a negligible potential increase after nearly 360 h of continuous operation, confirming

the much higher robustness compared with Ru@RuO_2 under acidic conditions. The excellent durability of Ru@Mn-RuO_2 heterostructure outperforms most of currently reported non-iridium-based acidic OER catalysts (Table S3). We used ICP-MS to examine the concentration of metallic ions in the electrolyte after chronopotentiometry stability test of Ru@Mn-RuO_2. The concentration of Ru ions in the electrolyte after electrolysis is 0.012 ppm, equivalent to 3.6wt% loss of Ru species, which is much smaller than that (22.1wt%) of Ru@RuO_2 after durability test. Furthermore, we systematically characterized post-catalysis Ru@Mn-RuO_2 heterostructure. The XRD pattern of Ru@Mn-RuO_2 catalyst after durability test clearly exhibits the tetragonal RuO_2 and hexagonal Ru phases (Figure S15) with no obvious changes on the crystal structure detected (Figure S16), and the slight shifts of Mn and Ru elements to lower binding energies (Figure S17) are probably ascribed to the tracing amount loss of RuO_2 species in Ru@Mn-RuO_2 catalyst during OER. The excellent OER stability of Ru@Mn-RuO_2 compared with pristine Ru@RuO_2 clearly indicates the critical role of Mn single-atom incorporation.

Electrolyzer performance

We further tested the performance of Ru@Mn-RuO_2 in electrolyzer platform to evaluate its potential for practical application. The as-assembled electrolyzer employing Ru@Mn-RuO_2 as the anode and commercial Pt/C as the cathode only requires 1.78 V to drive the current density of 1 A cm^{-2} (Figure 3h), which far outperforms the counterpart system using commercial RuO_2 as the anode. And the electrolyzer composed of Ru@Mn-RuO_2 || Com-Pt/C shows high stability without significant cell voltage increase during 20-h chronopotentiometry test at the current density of 250 mA cm^{-2} (Figure 3i), indicating the great potential of Ru@Mn-RuO_2 for practical hydrogen production in acidic media.

Mechanism understanding

We conducted DFT simulations to elucidate the influence of Mn dopants on the acidic OER performance, particularly focusing on the stability of RuO_2 catalyst. Based on our XRD observation, the RuO_2 crystals were modeled with a rutile lattice structure. Our choice of studying the catalytic properties of the fully oxidized (101) facet of RuO_2 stemmed from the exposed surface observed in Figure 1d-e. For our simulations, we adopted the (101) surface of tetragonal RuO_2, where the surface layer has 4 equivalent Ru atoms and one of them is substituted by a Mn dopant. This Mn-doped RuO_2 (101) surface was employed to investigate the impacts of Mn incorporation on the OER process. The schematic representation in Figure 4a illustrates a 4-electron OER process on Mn-doped RuO_2 (101), initiated by H_2O adsorption at a Ru site near the Mn dopant, followed by three sequential deprotonation steps to form $^*OH$,

*O, and then *OOH. The other two surface Ru sites were also tested but their energies for H_2O adsorption are 0.31 eV and 0.05 eV higher. Figure 4b presents the DFT-predicted free energy evolution for OER on both the pristine and Mn-doped RuO_2 (101) surfaces. The rate-determining step (RDS) for OER on both surfaces is found to be the transformation of *O to *OOH, aligning with previous results.[16,18,42-43]

The impacts of Mn incorporation on the OER activity and stability were evaluated by the RDS energy barrier and lattice stability calculations, respectively. The predicted RDS energy barrier for OER on the Mn-doped RuO_2 (101) surface (1.93 eV) is lower than that of the pure RuO_2 surface (2.01 eV), suggesting improved OER activity, in line with our experimental findings. The improved OER performance is explained by the projected density of states (PDOS) of the *d* orbitals of the Ru atom which interacts with the intermediates. As shown in Figure 4c, the *d*-band center shifts to lower energy level for Mn-doped RuO_2 surface, which is beneficial to increase the intrinsic activity for OER.[44-45] However, the remaining *d* electrons on the Ru cation decreased after Mn doping, as reflected in Figure S18 for the calculated electron density difference and the smaller Bader charge on the Ru cation for Mn-doped RuO_2 (12.10 e^-) compared to the pristine one (12.27 e^-) (Table S4). This suggest the *d*-band center shift for Mn-doped RuO_2 surface is caused by the change of PDOS profile. The reduced remaining *d* electrons in Mn-doped RuO_2 surface is likely from the increased charge transfer from Ru to O due to the shortened Ru-O bonds (Figure 4d) by crystal lattice contraction after Mn doping, consistent with the refined XRD and Ru-K edge EXAFS observations. The lattice contraction has been reported to induce a reduced reaction pathway, thus enhancing the catalytic activity and the stability.[46]

As for stability, we evaluated the enthalpy change for the surface Ru atom demetallation and subsurface oxygen loss from the surfaces of both RuO_2 (101) and Mn-RuO_2 (101). It is noted that the energies for Ru demetallation and oxygen loss are averaged over several configurations. The specific configurations and their corresponding energies can be found in Figure S19. Notably, the energy of Ru demetallation is much lower than that of oxygen loss, suggesting that Ru demetallation plays a key role in the stability of the RuO_2 surface. The incorporation of Mn into the lattice increased the energy cost for Ru demetallation from 1.57 to 2.06 eV (Figure 4e), indicating a more stable surface Ru in Mn-RuO_2 than in RuO_2 and explaining the less Ru dissolution from Mn-RuO_2 from the stability test. Our DFT simulations indicate that the incorporation of Mn improves both the OER activity and stability of RuO_2 by reducing RDS energy barrier and surface Ru demetallation, supporting our experimental observations of significantly enhanced OER performance of the Ru@Mn-RuO_2 catalyst.

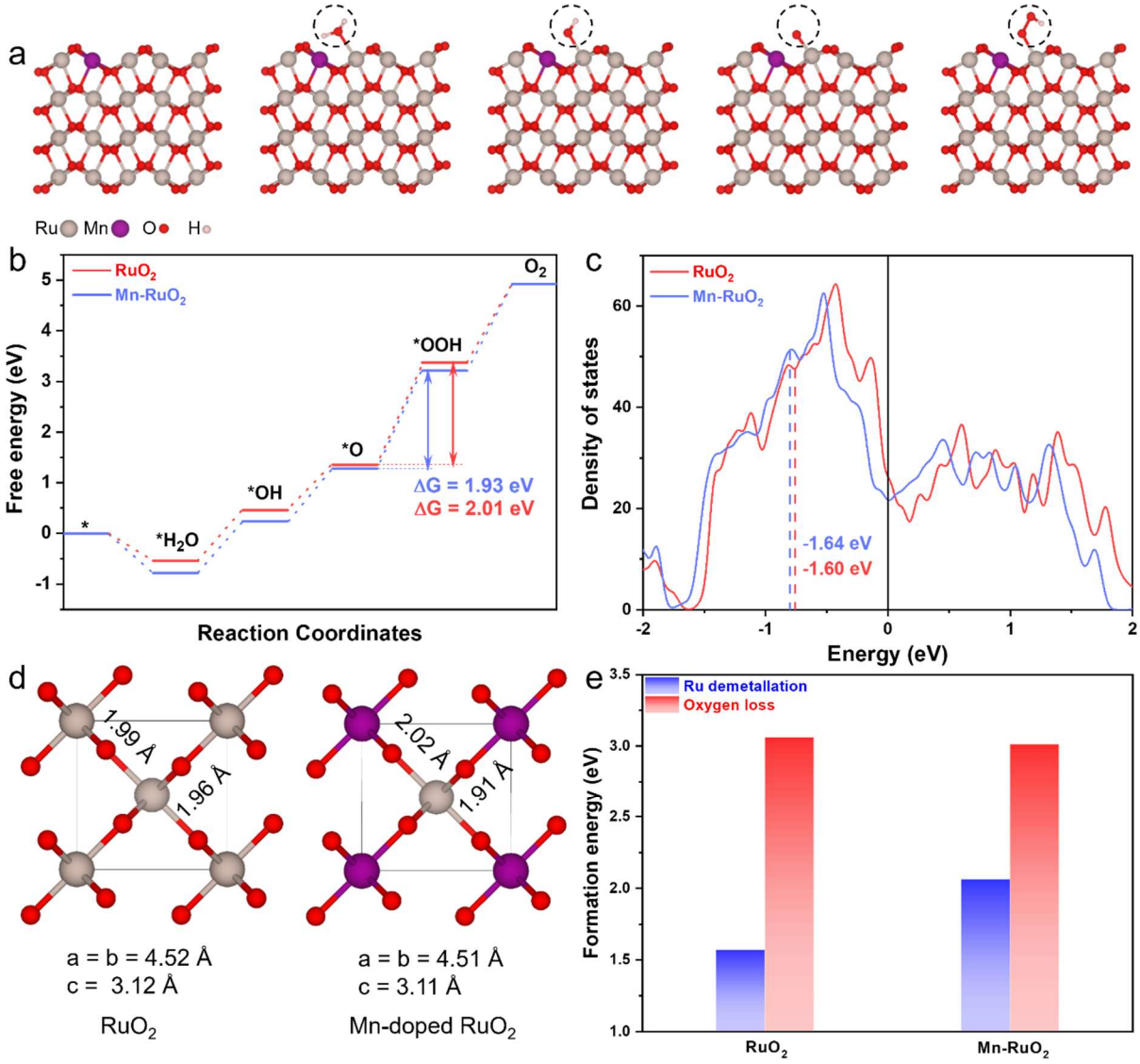

Figure 4. **Theoretical simulation results of the OER mechanism**. a, Atomic structures of the clean surface of Mn-RuO_2 (101) and the intermediate adsorption during OER process. Grey, purple, red and pink balls represent Ru, Mn, O and H atoms, respectively. The intermediates are highlighted in dashed circles. b. Free energy diagrams for OER on the RuO_2 (101) and Mn-RuO_2 (101) surfaces. c. Projected DOS and *d* band centers for RuO_2 (101) and Mn-RuO_2 (101) surfaces. d, Calculated lattice parameters of tetragonal RuO_2 (left) and Mn doped tetragonal RuO_2 (right) using DFT simulation technique. e, Calculated energies for structural degradation of RuO_2 (101) and Mn-RuO_2 (101) surfaces.

Apart from the MnO_x-Ru (oxide shell) synergy, we also constructed pristine and Mn doped Ru/RuO_2 interfaces (Figure S20) to investigate the effect of the MnO_x-Ru (metal core) synergy and Ru (core)-RuO_2 (shell) synergy on acidic OER activity and stability. The free energy diagram for OER in Figure S21 shows that the RDS on both interfaces is the transformation of *OOH to O_2,[47] rather than the transformation of *O to *OOH, which is ascribed to the promoted

adsorption strength of *OOH species in the existence of interfacial metallic Ru species. And both the energy gap of the last two steps narrowed after Mn doping in Ru/RuO_2 interface, i.e. decreased from 1.62 to 1.55 eV for the transformation of *O to *OOH, and from 1.86 to 1.79 eV for the transformation of *OOH to O_2, correspondingly. These four Gibbs free energy difference values are all much smaller than that marked in Figure 4b, and the calculated *d*-band center of Ru/Mn-RuO_2 interface in Figure S22 shifted to lower energy level from Fermi energy compared with that of Ru/RuO_2 interface with/without Mn doping, indicating the key role of MnO_x-Ru (metal core) synergy and Ru (core)-RuO_2 (shell) synergy for enhanced OER activity. As for stability investigation shown in Figure S23, improved formation energies of Ru cations de-metallization were achieved after Mn doping in the interface model, indicating the key role of multi-synergy effect on enhanced structural stability.

Conclusions

In summary, we have developed a Ru@Mn-RuO_2 core/shell heterostructure catalyst for high-performance acidic OER, in which Mn is atomically dispersed in RuO_2 shell. The incorporation of Mn single atoms induces lattice contraction of RuO_2 shell and modulates the electronic structure of active Ru cation, forming multiple synergistic effects including single atomic Mn with Ru species in RuO_2 shell, single atomic Mn with Ru species in Ru core, and the core/shell heterostructure itself, thus efficiently reducing the RDS energy barrier of OER and resisting the overoxidation of RuO_2 active sites during acidic electrocatalytic process. Consequently, the Ru@Mn-RuO_2 heterostructure exhibited much improved activity and stability towards acidic OER compared with the undoped Ru@RuO_2. This finding paves the way to construct heterostructures with multiple synergistic effects for the energy/environment-related electrocatalytic applications. The encouraging performance we have achieved using single-atom doped core/shell Ru@Mn-RuO_2 heterostructure suggests the future potential of replacing high-cost iridium-based catalysts.

Supporting Information

Supplementary Information is available from the Wiley Online Library or from the author.

Acknowledgements

This work was financially supported from the Natural National Science Foundation of China (No.22179098). The authors sincerely acknowledge the Spherical Aberration Corrected Transmission Electron Microscope characterization test support from Dalian Institute of Chemical Physics, Chinese Academy of Sciences, China. The authors also acknowledge the X-ray absorption spectroscopy test support from Beijing Synchrotron Radiation Faciality, Chinese

Academy of Sciences, China. We acknowledge the National Supercomputing Centre of Singapore (NSCC) for providing computing resources.

Author Contributions

H. Ma, H. Cheng and J. Ma conceived the research project. H. Cheng and J. Ma supervised the project. H. Ma designed the catalysts, performed most of experimental section and conducted detailed analysis of the experimental data. J. Zhou performed the density functional theory simulations and provided solid evidence to explain the experimental findings. Y. Zhao conducted the spherical aberration corrected transmission electron microscope test and analyzed the relevant characterization results in detail. Z. Hu provided much insightful advices and contributed a lot to unearth the physics merits of the extraordinary structure and its relevance to the high catalytic performances.